Electronic supplementary information (ESI)

Crystallographic Characterization of $Er_2C_2@C_2(43)$-C_{90}, $Er_2C_2@C_2(40)$-C_{90}, $Er_2C_2@C_2(44)$-C_{90}, and $Er_2C_2@C_1(21)$-C_{90} Isomers: The Role of Cage-Shape on Cluster Configuration

Shuaifeng Hu,‡[a] Wangqiang Shen,‡[a] Pei Zhao,‡[b,c] Ting Xu,[a] Zdeněk Slanina,[a] Masahiro Ehara,[c] Xiang Zhao,*[,b] Yunpeng Xie,*[,a] Takeshi Akasaka,*[,a] and Xing Lu*[,a]

[a] *State Key Laboratory of Materials Processing and Die & Mould Technology, School of Materials Science and Engineering, Huazhong University of Science and Technology, 1037 Luoyu Road, Wuhan, 430074, China. E-mail: lux@hust.edu.cn*

[b] *Institute for Chemical Physics & Department of Chemistry, State Key Laboratory of Electrical Insulation and Power Equipment, School of Science, Xi'an Jiaotong University, Xi'an 710049, China. E-mail: xzhao@mail.xjtu.edu.cn*

[c] *Research Center for Computational Science, Institute for Molecular Science, Okazaki, 444-8585, Japan. E-mail: ehara@ims.ac.jp*

Table of Contents

carbide clusters of $Er_2C_2@C_2(43)$-C_{90}, $Er_2C_2@C_2(40)$-C_{90}, $Er_2C_2@C_2(44)$-C_{90}, and $Er_2C_2@C_1(21)$-C_{90}.

Table S4-S7. Cage screening and relative energy analysis for Er_2C_{92} isomers.

Table S8. The natural electron configuration of $Er_2C_2@C_{90}$ isomers.

Table S9. BCP parameters and delocalization indices (DI) for the Er-C and C-C bonds in $Er_2C_2@C_{90}$ isomers.

Table S10. The details of the vis-NIR absorptions of $Er_2C_2@C_{90}$ isomers.

Fig. S4 Low-energy Raman spectra of $Er_2C_2@C_{90}$ isomers.

Fig. S5 Stone-Wales transformations among the eight reported C_{90} cags.

Fig. S6 PL spectra of the $Er_2C_2@C_{90}$ isomers.

Fig. S7 Cyclic voltammograms of $Er_2C_2@C_{90}$ isomers.

Fig. S8 DPV curves of $Er_2C_2@C_2(43)$-C_{90}, $Er_2C_2@C_2(40)$-C_{90}, $Er_2C_2@C_2(44)$-C_{90}, and $Er_2C_2@C_1(21)$-C_{90}.

References.

General characterization. HPLC was conducted on an LC-908 machine (Japan Analytical Industry Co., Ltd.) with toluene/chlorobenzene as mobile phase. LDI-TOF mass spectrometry was measured on a BIFLEX III spectrometer (Bruker Daltonics Inc., Germany). Vis-NIR absorption spectra were measured on a LAMBDA 750 UV/vis/NIR spectrophotometer (PerkinElmer, US) in carbon disulfide at room temperature. The Raman and photoluminescence (PL) spectra were excited with 532 nm radiation of an Nd-YAG laser on a Horiba LabRAM HR800 spectrometer in ambient condition. CV results were obtained in o-dichlorobenzene using a CHI-660E instrument. A conventional three-electrode cell consisting of a platinum counter electrode, a glassy carbon working electrode, and a silver reference electrode was used for all measurements. $TBAPF_6$ (0.05 M) was used as the supporting electrolyte. At the end of the experiments, ferrocene was added as an internal reference for measuring the potentials. The CVs were measured at a scan rate of 100 mV s^{-1} at room temperature under nitrogen protection.

Preparation and isolation of $Er_2C_2@C_2(43)$-C_{90}, $Er_2C_2@C_2(40)$-C_{90}, $Er_2C_2@C_2(44)$-C_{90},

and $Er_2C_2@C_1(21)$-C_{90}. Soot containing erbium-EMFs was synthesized using a direct-current arc discharge method.[1] The graphite rods packed with Er_2O_3/graphite powder (molar ratio of Er/C= 1:15) was annealed and then vaporized in the arcing chamber under a 250 Torr helium atmosphere with a power of 110 A × 30 V. Then, the as-produced fullerene soot was collected and sonicated in carbon disulfide for 1 h under argon atmosphere. After solvent removal, the extracted fullerenes were dissolved in toluene and the solution was subjected to HPLC separations. Further details are described below.

Single-crystal XRD measurements of $Er_2C_2@C_2(43)$-C_{90}, $Er_2C_2@C_2(40)$-C_{90}, $Er_2C_2@C_2(44)$-C_{90}, and $Er_2C_2@C_1(21)$-C_{90}. Crystalline blocks of $Er_2C_2@C_{90}$ isomers were obtained by layering a benzene solution of Ni^{II}(OEP) over a nearly saturated solution of the EMFs in CS_2 in a glass tube at 0 °C. Over a 20-day period, the two solutions diffused together and black crystals formed on the wall and at the bottom of the tube. Single-crystal XRD measurements of $Er_2C_2@C_2(43)$-C_{90}, $Er_2C_2@C_2(40)$-C_{90}, and $Er_2C_2@C_1(21)$-C_{90} were performed at 100 K using synchrotron radiation (λ= 0.82654) with a MarCCD detector at beamline BL17B station of Shanghai Synchrotron Radiation Facility.[2] Crystallographic characterization of $Er_2C_2@C_2(44)$-C_{90} was performed at 150 K on a Bruker D8 QUEST diffractometer using Cu K_α radiation (λ= 1.54178 Å) (Bruker AXS Inc., Germany). The Multi-Scan method (SADABS) was used for absorption corrections. The structures were solved by direct method and were refined with *SHELXL-2018/1*.[3] CCDC-1916262 ($Er_2C_2@C_2(43)$-C_{90}), CCDC-1916263 ($Er_2C_2@C_2(40)$-C_{90}), CCDC-1916264 ($Er_2C_2@C_2(44)$-C_{90}), and CCDC-1916265 ($Er_2C_2@C_1(21)$-C_{90}) contain the supplementary crystallographic data for this paper. These data can be obtained free of charge from The Cambridge Crystallographic Data Centre via www.ccdc.cam.ac.uk/data_request/cif.

Computational details. There are 46 and 86 IPR isomers for C_{90} and C_{92}, respectively. Optimizations on C_{90}^{2-}, C_{90}^{4-}, C_{92}^{4-}, and C_{92}^{6-} anions of these IPR isomers were performed at B3LYP[4-6] with a split valence d-polarized 6-31G* basis set (the results are shown in Tables S4 and S5). $C_2(41)$-C_{90} is the most stable C_{90}^{4-} isomer, and the following four most stable C_{90}^{4-} isomers are $C_2(43)$-C_{90}, $C_2(44)$-C_{90}, $C_2(40)$-C_{90}, and $C_1(21)$-C_{90}. The

latter four isomers correspond to the four isomers obtained in experiments, indicative of the four electrons transfer from the metallic cluster to the cage. As a contrast, the C_{90}^{2-} isomers exhibit rather different energy trends, which do support the four isomers disclosed in $Sm^{2+}@C_{90}^{2-}$ series very well.[7] The previous report also revealed that four electrons are formally transferred from the Er_2C_2 cluster to the fullerene cage,[8] therefore, the 15 most stable C_{90}^{4-} isomers with relative energies lower than 26 kcal/mol were taken into account to encapsulate the Er_2C_2 cluster. However, the Er_2 cluster may transfer four or six electrons to the fullerene cages. Consequently, 24 C_{92} isomers including 22 isomers with relative energies lower than 20 kcal/mol at the tetra-anion state and 2 isomers (C_2(61)-C_{92} and T(86)-C_{92}) with low relative energies at hexa-anion state were considered for $Er_2@C_{92}$. The corresponding Er_2C_{92} isomers were optimized at UB3LYP with basis sets of 3-21G (for C) and the Stuttgart/Dresden (SDD) basis set[9] with the ECP28MWB_SEG core potential (for Er).[10-11] Further optimization on 8 $Er_2@C_{92}$ isomers and 14 $Er_2C_2@C_{90}$ isomers were carried out at the UB3LYP/6-31G(d)-SDD~ECP28MWB_SEG level of theory. Harmonic frequency analyses were carried out at the level of UB3LYP/3-21G-SDD~ECP28MWB_SEG to verify that the stationary points are local minima on the potential energy surface. Based on the frequency analyses, rotational-vibrational partition functions were obtained to evaluate the molar fractions of the Er_2C_{92} series at elevated temperatures. Although the partition functions are constructed within the rigid-rotor and harmonic-oscillator approach, it can be expected that anharmonicity corrections should substantially cancel out.[12] Previous studies have demonstrated that the entropy contributions play a critical role in the stabilization of endohedral fullerene isomers.[13-16] All $Er_2C_2@C_{90}$ and $Er_2@C_{92}$ isomers were optimized in their septet ground state. In addition, natural electron configuration analyses were obtained by single-point energy calculation at the level of B3LYP/6-311G(d, p)-SDD~ECP28MWB_SEG. All DFT calculations were carried out using the Gaussian 09 program package.[17]

High-performance liquid chromatography (HPLC) separation processes of $Er_2C_2@C_{90}$ isomers. The first stage was performed on a 5PYE column (20 mm × 250 mm, Cosmosil Nacalai Tesque) with toluene as mobile phase. Fig. S1a shows the corresponding

chromatogram. The region of the collected component containing $Er_2C_2@C_{90}$ isomers is highlighted with colored shadows. The last fraction, which is named as Fr8, was collected. After that, Fr8 was injected into a 5PBB column (20 mm × 250 mm, Cosmosil Nacalai Tesque) for the second stage separation using chlorobenzene as eluent, and Fr84 was obtained (Fig. S1b). Then, Fr84 was injected into a Buckyprep-M column (20 mm × 250 mm, Cosmosil Nacalai Tesque) using chlorobenzene as eluent, and Fr842 was obtained (Fig. S1c). Fr842 was then injected into a Buckyprep column (20 mm × 250 mm, Cosmosil Nacalai Tesque) using chlorobenzene as the eluent, and Fr8423 was obtained (Fig. S1d). As for Fr8423, a 5PBB column (10 mm × 250 mm, Cosmosil Nacalai Tesque) was used for the separation, and Fr84232 was collected (Fig. S2a). After that, Fr84232 was injected into a Buckyprep column (20 mm × 250 mm, Cosmosil Nacalai Tesque), and three fractions, named Fr842321, Fr842322, and Fr842323, were collected, respectively, in which Fr842323 represents the pure compound of $Er_2C_2@C_1(21)$-C_{90} (Fig. S2b). However, Fr842321 was injected into a Buckyprep column (20 mm × 250 mm, Cosmosil Nacalai Tesque) using chlorobenzene as the eluent, then Fr8423211 ($Er_2C_2@C_2(43)$-C_{90}) and Fr8423212 ($Er_2C_2@C_2(40)$-C_{90}) were obtained with high purity (Fig. S2c). As for Fr842322, a Buckyprep-M column (20 mm × 250 mm, Cosmosil Nacalai Tesque) was used for the last stage separation, and Fr8423222 ($Er_2C_2@C_2(44)$-C_{90}) was obtained eventually (Fig. S2d).

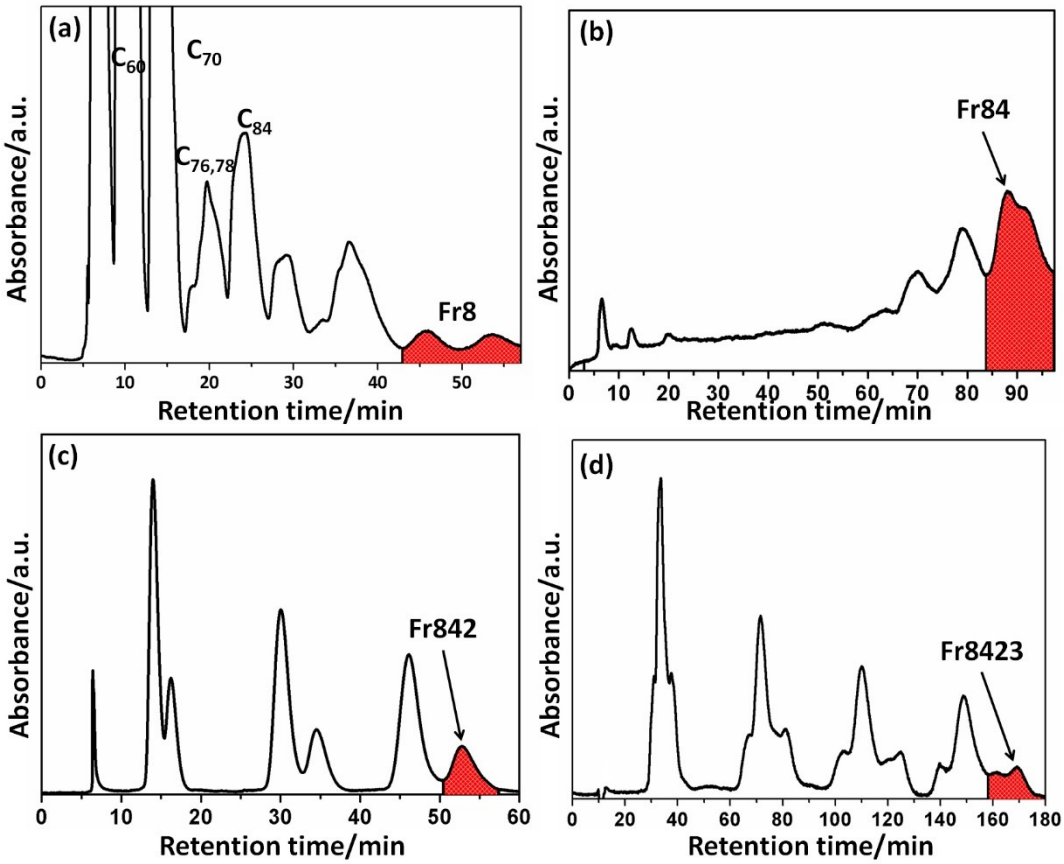

Fig. S1 (a) Isolation scheme of fullerene extract on a 5PYE column. Conditions: eluent: toluene, 10 mL/min flow rate; inject volume: 20 mL; (b) Isolation scheme of Fr8 on a 5PBB column. Conditions: eluent: chlorobenzene, 10 mL/min flow rate; inject volume: 20 mL; (c) Recycling HPLC chromatogram of Fr84 on a Buckyprep-M column. Conditions: 10 mL injection volume; 10 mL/min chlorobenzene flow. (d) Recycling HPLC chromatogram of Fr842 on a Buckyprep column. Conditions: 10 mL injection volume; 6 mL/min chlorobenzene flow. (All of the detection wavelengths are 330 nm.)

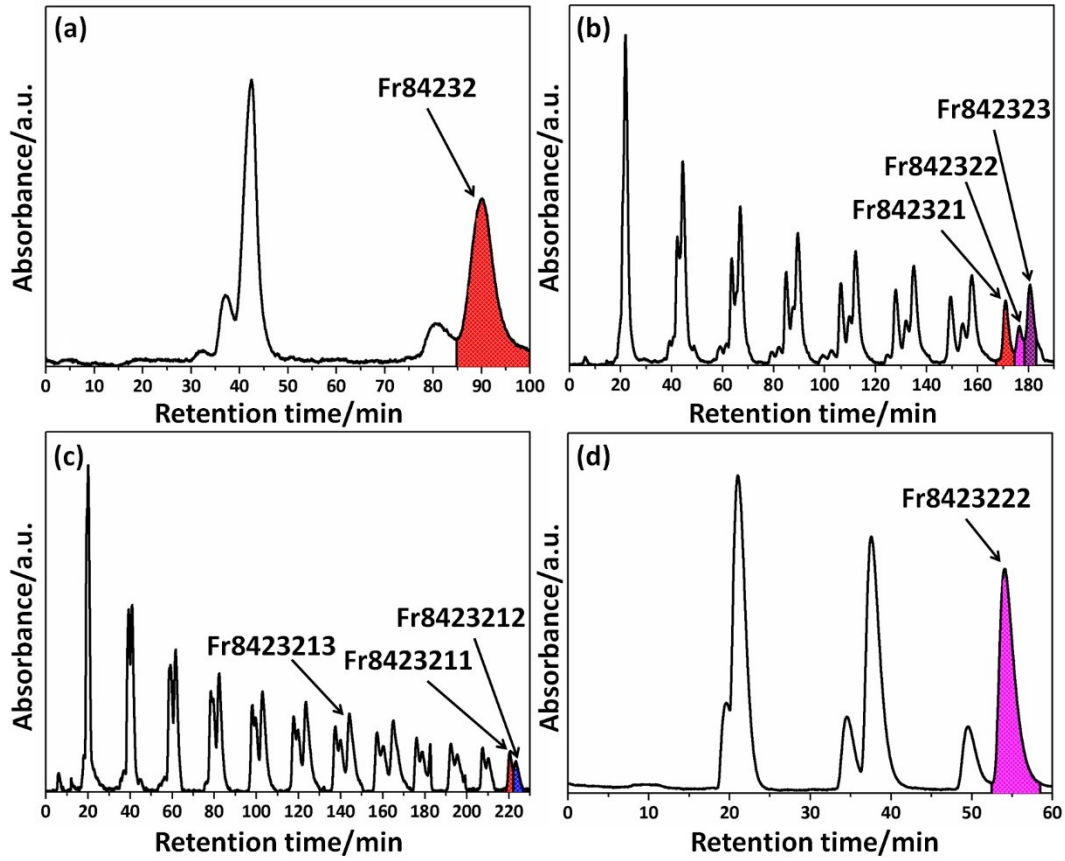

Fig. S2 (a) Recycling HPLC chromatogram of Fr8423 on a 5PBB column. Conditions: 10 mL injection volume; 5 mL/min chlorobenzene flow; (b) Recycling HPLC chromatogram of Fr84232 on a Buckyprep column. Conditions: 10 mL injection volume; 10 mL/min chlorobenzene flow; (c) Recycling HPLC chromatogram of Fr842321 on a Buckyprep column and Fr8423213 was removed step by step. Conditions: 10 mL injection volume; 10 mL/min chlorobenzene flow. (d) Recycling HPLC chromatogram of Fr842322 on a Buckyprep-M column. Conditions: 15mL injection volume; 10 mL/min chlorobenzene flow. (All of the detection wavelengths are 330 nm.)

Table S1. Crystallographic data of $Er_2C_2@C_2(43)$-C_{90}·Ni^{II}(OEP), $Er_2C_2@C_2(40)$-C_{90}·Ni^{II}(OEP), $Er_2C_2@C_2(44)$-C_{90}·Ni^{II}(OEP), and $Er_2C_2@C_1(21)$-C_{90}·1.5Ni^{II}(OEP).

Compound	$Er_2C_2@C_2(43)$-C_{90}• Ni^{II}(OEP)•2(C_6H_6)	$Er_2C_2@C_2(40)$-C_{90}• Ni^{II}(OEP)	$Er_2C_2@C_2(44)$-C_{90}• Ni^{II}(OEP)•(C_6H_6)	2[$Er_2C_2@C_1(21)$-C_{90}]• 3Ni^{II}(OEP) •2(C_6H_6)
T, K	100(2)	100(2)	150(2)	100(2)
λ, Å	0.82654	0.82654	1.54178	0.82654
color/habit	black / block	black / block	black / block	black / block
crystal size, mm	0.26×0.20×0.12	0.22×0.18×0.10	0.21×0.18×0.13	0.20×0.13×0.1
Empirical formula	$C_{140}H_{56}Er_2N_4Ni$	$C_{128}H_{44}Er_2N_4Ni$	$C_{134}H_{50}Er_2N_4Ni$	$C_{304}H_{144}Er_2N_{12}Ni_3$
fw	2187.06	2030.75	2108.99	4809.46
crystal system	monoclinic	monoclinic	monoclinic	monoclinic
space group	*C*2/*m*	*C*2/*m*	*C*2/*m*	*C*2/*m*
a, Å	24.4039(9)	24.3837(6)	24.2849(17)	24.7746(8)
b, Å	17.9573(7)	17.8891(5)	18.2618(13)	17.6929(6)
c, Å	18.9278(8)	18.9805(5)	18.5731(13)	23.2522(7)
α, deg	90.000	90.000	90.000	90.000
β, deg	90.465(1)	90.101(1)	91.612(3)	103.045(1)
γ, deg	90.000	90.000	90.000	90.000
V, Å³	8294.4(6)	8279.3(4)	8233.7(10)	9929.2(6)
Z	4	4	4	2
ρ, g/cm³	1.751	1.629	1.701	1.609
μ, mm^{-1}	3.391	3.387	4.418	2.982
Data/restraints/parameter	7868/4689/1241	7778/1423/1202	8578/1957/1232	8580/1766/1354
R1[reflections with I>2σ(I)]	0.1059 (5687)	0.1131 (6223)	0.1084 (7164)	0.0775 (6675)
wR2 (all data)	0.3130	0.2965	0.3296	0.2531

Table S2. The fractional occupancies of the Er positions in $Er_2C_2@C_{90}$ isomers.

EMFs	Fractional occupancy of the Er positions[a]										
$Er_2C_2@C_2(43)$-C_{90}	Er1/	Er2/	Er3/	Er4/	Er5/	Er6/	Er7	Er8/	Er9/	Er10/	Er11/
	Er1A	Er2A	Er3A	Er4A	Er5A	Er6A		Er8A	Er9A	Er10A	Er11A
	0.15	0.11	0.11	0.11	0.10	0.10	0.07	0.05	0.04	0.04	0.04
	Er12/	Er13	Er14/	Er15/	Er16/						
	Er12A		Er14A	Er15A	Er16A						
	0.03	0.03	0.03	0.03	0.02						
$Er_2C_2@C_2(40)$-C_{90}	Er1/	Er2/	Er3/	Er4/	Er5/	Er6/	Er7/	Er8/	Er9/	Er10/	Er11
	Er1A	Er2A	Er3A	Er4A	Er5A	Er6A	Er7A	Er8A	Er9A	Er10A	
	0.29	0.16	0.06	0.05	0.04	0.04	0.04	0.04	0.04	0.03	0.03
	Er12	Er13	Er14/	Er15/	Er16	Er17/	Er18/	Er19/	Er20/	Er21/	Er22/
			Er14A	Er15A		Er17A	Er18A	Er19A	Er20A	Er21A	Er22A
	0.03	0.02	0.02	0.02	0.02	0.02	0.02	0.02	0.02	0.02	0.02
$Er_2C_2@C_2(44)$-C_{90}	Er1	Er2/	Er3/	Er4/	Er5/	Er6/	Er7	Er8/	Er9/	Er10/	Er11/
		Er2A	Er3A	Er4A	Er5A	Er6A		Er8A	Er9A	Er10A	Er11A
	0.37	0.21	0.15	0.11	0.11	0.08	0.04	0.03	0.03	0.02	0.02
	Er12	Er13/	Er14/	Er15							
		Er13A	Er14A								
	0.02	0.01	0.01	0.01							
$Er_2C_2@C_1(21)$-C_{90}	Er1/	Er2/	Er3/	Er4/	Er5/	Er6/	Er7/	Er8/	Er9/	Er10/	Er11/
	Er1A	Er2A	Er3A	Er4A	Er5A	Er6A	Er7A	Er8A	Er9A	Er10A	Er11A
	0.20	0.12	0.11	0.08	0.07	0.05	0.05	0.05	0.04	0.04	0.04
	Er12	Er13/	Er14	Er15/	Er16/	Er17/	Er18/				
		Er13A		Er15A	Er16A	Er17A	Er18A				
	0.04	0.04	0.02	0.03	0.02	0.02	0.01				

[a]The atom with a suffix 'A' is generated by the crystallographic operation.

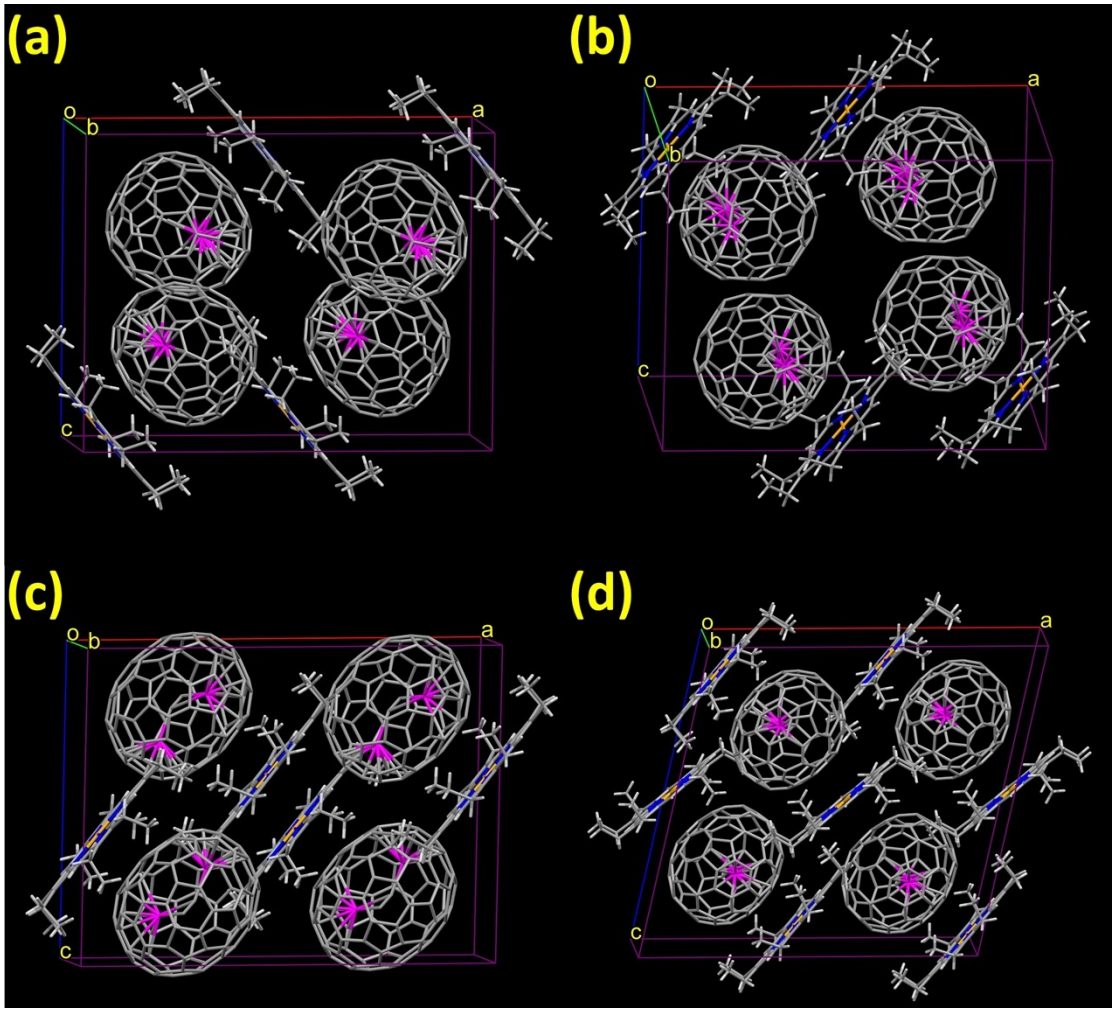

Fig. S3 Packing structures of (a) Er_2C_2@C_2(43)-C_{90}·Ni^{II}(OEP), (b) Er_2C_2@C_2(40)-C_{90}·Ni^{II}(OEP), (c) Er_2C_2@C_2(44)-C_{90}·Ni^{II}(OEP), and (d) Er_2C_2@C_1(21)-C_{90}·1.5Ni^{II}(OEP) with minor disordered components and solvents omitted for clarity.

Table S3. Cage size, L_a/L_b ratio, Er···cage distance, Ni···cage distance, details of the carbide clusters of $Er_2C_2@C_2(43)$-C_{90}, $Er_2C_2@C_2(40)$-C_{90}, $Er_2C_2@C_2(44)$-C_{90}, and $Er_2C_2@C_1(21)$-C_{90}. (L_a: length of major axis of the cage, L_b: length of minor axis of the cage)

Compound[a]	L_a (Å)	L_b (Å)	L_a/L_b ratio	Er···Er distance (Å)	C-C (carbide) (Å)	Er···C distance (carbide) (Å)	Er_2C_2 dihedral angle	Shortest Er-cage distance (Å)	Shortest Ni-cage distance (Å)
$Er_2C_2@C_2(43)$-C_{90}	8.723	7.721	1.129	3.927	1.044	2.405-2.412	174.5°	2.026	2.954
$Er_2C_2@C_2(40)$-C_{90}	8.923	7.608	1.173	4.058	1.036	2.205-2.565	136.7°	2.034	2.912
$Er_2C_2@C_2(44)$-C_{90}	9.054	7.412	1.222	4.172	0.984	1.994-2.723	117.8°	2.194	2.977
$Er_2C_2@C_1(21)$-C_{90}	9.169	7.491	1.224	4.651	0.944	2.484-2.577	140.1°	2.091	2.994/2.964

[a]The major Er_2C_2 cluster and the prominent fullerene cage in these EMFs.

Table S4. Relative energies (ΔE, in kcal/mol) of C_{90}^{4-} and C_{90}^{2-} at the level of B3LYP/6-31G*.

No.	IPR No.	Spiral No.	Sym.	C_{90}^{4-}	C_{90}^{2-}
				ΔE	ΔE
1	41	99913	C_2	0.0	2.6
2	43	99915	C_2	2.5	7.3
3	44	99916	C_2	7.6	9.2
4	40	99912	C_2	8.4	0.1
5	21	99893	C_1	9.9	13.6
6	10	99882	C_s	10.7	10.7
7	42	99914	C_2	14.3	0.0
8	45	99917	C_2	15.3	0.4
9	23	99895	C_2	15.5	11.1
10	35	99907	C_s	21.9	12.1
11	36	99908	C_{2v}	23.4	20.8
12	38	99910	C_1	24.4	14.5
13	22	99894	C_1	24.5	7.5
14	46	99918	C_{2v}	25.3	7.0
15	19	99891	C_2	25.3	16.5
16	20	99892	C_1	26.8	10.3
17	9	99881	C_1	27.6	11.4
18	30	99902	C_1	28.4	15.9
19	28	99900	C_2	29.7	19.8
20	32	99904	C_1	30.1	18.3
21	26	99898	C_1	32.3	19.8

22	8	99880	C_2	38.5	26.1
23	7	99879	C_1	41.2	18.3
24	24	99896	C_1	41.5	28.8
25	11	99883	C_1	43.3	24.3
26	18	99890	C_2	43.4	18.2
27	25	99897	C_{2v}	44.6	44.8
28	6	99878	C_2	44.9	16.7
29	29	99901	C_1	45.5	27.6
30	5	99877	C_s	47.4	39.1
31	12	99884	C_2	48.8	38.1
32	27	99899	C_1	51.0	29.7
33	37	99909	C_2	52.2	20.6
34	31	99903	C_2	54.8	40.9
35	4	99876	C_2	55.8	24.3
36	33	99905	C_s	58.7	39.1
37	17	99889	C_s	60.8	39.6
38	15	99887	C_1	62.1	41.4
39	13	99885	C_{2v}	64.8	39.7
40	34	99906	C_s	65.2	35.2
41	39	99911	C_{2v}	65.5	48.3
42	14	99886	C_1	69.3	44.0
43	3	99875	C_1	71.2	44.1
44	1	99873	D_{5h}	75.5	46.7
45	2	99874	C_{2v}	96.2	71.7
46	16	99888	C_{2v}	101.9	72.3

Table S5. Relative energies (ΔE, in kcal/mol) of C_{92}^{4-} and C_{92}^{6-} at the level of B3LYP/6-31G*.

No.	IPR No.	Spiral No.	Sym.	C_{92}^{4-}	C_{92}^{6-}
				ΔE	ΔE
1	85	126408	D_3	0.0	0.0
2	64	126387	C_2	7.0	10.2
3	67	126390	C_1	7.3	19.6
4	16	126339	C_s	10.1	16.0
5	66	126389	C_1	10.8	5.4
6	59	126382	C_1	12.0	17.2
7	36	126359	C_2	13.5	14.3
8	69	126392	C_2	14.6	23.5
9	74	126397	C_2	14.7	22.9
10	68	126391	C_1	15.0	15.4
11	32	126355	C_1	16.0	22.0
12	44	126367	C_1	16.1	13.3
13	60	126383	C_1	16.5	17.8

14	15	126338	C_s	16.7	23.4
15	75	126398	C_2	16.7	17.5
16	77	126400	C_2	17.0	11.8
17	70	126393	C_1	17.2	22.5
18	76	126399	C_1	17.6	24.7
19	65	126388	C_2	17.6	7.5
20	62	126385	C_1	18.2	25.3
21	10	126333	C_1	19.3	23.6
22	31	126354	C_2	19.9	31.9
23	73	126396	C_1	20.5	27.5
24	61	126384	C_2	20.6	15.0
25	63	126386	C_1	21.5	22.1
26	24	126347	C_s	22.8	28.1
27	42	126365	C_1	22.9	25.0
28	80	126403	C_2	23.2	33.3
29	34	126357	C_2	23.7	20.5
30	43	126366	C_1	25.3	27.7
31	72	126395	C_1	25.6	21.6
32	84	126407	D_2	25.9	18.7
33	81	126404	D_2	26.4	28.1
34	55	126378	C_1	28.0	35.5
35	79	126402	C_2	28.9	32.1
36	86	126409	T	29.1	6.1
37	9	126332	C_2	29.5	39.8
38	71	126394	D_3	29.9	19.7
39	38	126361	C_1	29.9	24.8
40	82	126405	D_2	30.0	26.2
41	83	126406	D_3	30.3	22.7
42	11	126334	C_1	31.5	40.5
43	58	126381	C_1	32.3	39.5
44	47	126370	C_1	32.4	26.9
45	46	126369	C_2	32.6	27.4
46	78	126401	D_3	32.7	30.5
47	56	126379	C_1	32.9	37.7
48	53	126376	C_1	33.4	41.2
49	57	126380	C_1	34.7	37.6
50	12	126335	C_1	34.8	38.1
51	50	126373	C_1	36.7	45.0
52	27	126350	C_2	36.7	42.1
53	52	126375	C_1	37.4	46.3
54	54	126377	C_1	39.8	48.5
55	8	126331	C_1	40.4	49.8
56	33	126356	C_1	40.5	46.7
57	23	126346	C_2	40.9	50.6

58	26	126349	C_2	41.2	44.9
59	30	126353	C_1	41.4	43.9
60	40	126363	C_1	42.9	53.0
61	39	126362	C_1	43.1	47.3
62	14	126337	C_s	43.7	46.9
63	19	126342	C_2	44.1	43.2
64	18	126341	C_1	44.7	47.4
65	41	126364	C_3	46.5	48.1
66	48	126371	C_2	47.4	54.8
67	35	126358	C_{2v}	49.5	45.4
68	13	126336	C_1	49.9	55.3
69	45	126368	C_s	50.0	44.0
70	28	126351	D_3	53.7	55.2
71	25	126348	C_2	54.4	55.4
72	6	126329	C_s	54.9	60.6
73	49	126372	C_2	58.8	63.5
74	51	126374	C_2	59.3	67.3
75	5	126328	C_s	59.5	68.1
76	2	126325	C_1	59.5	66.5
77	37	126360	C_1	60.0	67.8
78	7	126330	C_2	60.1	68.8
79	4	126327	C_2	60.6	67.1
80	29	126352	D_{2h}	62.5	70.8
81	20	126343	C_1	64.2	66.0
82	17	126340	C_2	67.7	73.1
83	21	126344	C_s	84.5	66.0
84	1	126324	D_2	90.9	96.0
85	22	126345	C_{2v}	91.4	93.1
86	3	126326	C_2	91.9	98.9

Table S6. Relative energies (ΔE, in kcal/mol) and HOMO-LUMO gaps (in eV) of $Er_2C_2@C_{90}$ and $Er_2@C_{92}$ at the level of UB3LYP/3-21G-SDD~ECP28MWB_SEG (septet). Isomers obtained by crystallographic studies are marked in bold.

EMF	IPR No.	Spiral No.	Sym.	ΔE	Gap
$Er_2C_2@C_{90}$	**43**	**99915**	**C_2**	**0.0**	**1.33**
$Er_2@C_{92}$	36	126359	C_2	2.0	0.82
$Er_2C_2@C_{90}$	46	99918	C_{2v}	2.1	1.46
$Er_2@C_{92}$	85	126408	D_3	2.2	0.67
$Er_2C_2@C_{90}$	41	99913	C_2	2.4	1.49
$Er_2C_2@C_{90}$	**40**	**99912**	**C_2**	**2.5**	**1.46**
$Er_2@C_{92}$	15	126338	C_s	3.4	1.09
$Er_2@C_{92}$	32	126355	C_1	3.8	0.86
$Er_2C_2@C_{90}$	42	99914	C_1	4.4	1.09

$Er_2@C_{92}$	64	126387	C_2	4.5	0.84
$Er_2@C_{92}$	16	126339	C_s	7.5	0.83
$Er_2@C_{92}$	67	126390	C_1	7.6	0.77
$Er_2@C_{92}$	60	126383	C_1	8.0	0.88
$Er_2C_2@C_{90}$	**21**	**99893**	**C_1**	**8.7**	**1.40**
$Er_2@C_{92}$	10	126333	C_1	9.3	0.88
$Er_2@C_{92}$	70	126393	C_1	9.6	1.19
$Er_2C_2@C_{90}$	22	99894	C_1	9.8	1.11
$Er_2@C_{92}$	77	126400	C_2	10.3	0.79
$Er_2@C_{92}$	44	126367	C_1	10.6	0.94
$Er_2@C_{92}$	68	126391	C_1	10.6	0.84
$Er_2@C_{92}$	31	126354	C_2	11.2	1.17
$Er_2@C_{92}$	59	126382	C_1	12.0	0.83
$Er_2C_2@C_{90}$	23	99895	C_2	12.3	1.29
$Er_2@C_{92}$	76	126399	C_1	12.4	1.06
$Er_2C_2@C_{90}$	45	99917	C_2	13.1	1.12
$Er_2@C_{92}$	65	126388	C_2	13.5	0.94
$Er_2@C_{92}$	66	126389	C_1	13.9	0.80
$Er_2C_2@C_{90}$	10	99882	C_s	14.2	1.06
$Er_2C_2@C_{90}$	36	99908	C_{2v}	16.1	1.03
$Er_2C_2@C_{90}$	19	99891	C_2	16.1	0.81
$Er_2C_2@C_{90}$	38	99910	C_1	16.4	1.11
$Er_2@C_{92}$	61	126384	C_2	16.9	1.05
$Er_2C_2@C_{90}$	**44**	**99916**	**C_2**	**17.0**	**0.85**
$Er_2@C_{92}$	74	126397	C_2	18.9	0.98
$Er_2@C_{92}$	62	126385	C_1	18.9	0.94
$Er_2@C_{92}$	75	126398	C_2	19.5	0.81
$Er_2C_2@C_{90}$	35	99907	C_s	21.7	0.84
$Er_2@C_{92}$	69	126392	C_2	21.7	1.07
$Er_2@C_{92}$	86	126409	T	28.3	1.03

Table S7. Relative energies (ΔE, in kcal/mol) and HOMO-LUMO gaps (Gap, in eV) of $Er_2C_2@C_{90}$ and $Er_2@C_{92}$ at the level of UB3LYP/6-31G*-SDD~ECP28MWB_SEG (septet). Isomers obtained by crystallographic studies are marked in bold.

EMF	IPR No.	Spiral No.	Sym.	ΔE	Gap
$Er_2@C_{92}$	64	126387	C_2	0.0	0.97
$Er_2@C_{92}$	85	126408	D_3	2.0	0.95
$Er_2@C_{92}$	67	126390	C_1	2.6	0.76
$Er_2@C_{92}$	60	126383	C_1	4.0	1.00
$Er_2@C_{92}$	36	126359	C_2	4.4	0.82
$Er_2@C_{92}$	15	126338	C_s	6.5	1.20
$Er_2@C_{92}$	32	126355	C_1	7.8	0.85

$Er_2C_2@C_{90}$	41	99913	C_2	10.9	1.48
$Er_2C_2@C_{90}$	**40**	**99912**	**C_2**	**12.2**	**1.38**
$Er_2C_2@C_{90}$	**43**	**99915**	**C_2**	**13.2**	**1.29**
$Er_2C_2@C_{90}$	42	99914	C_1	15.4	1.12
$Er_2C_2@C_{90}$	46	99918	C_{2v}	16.8	1.40
$Er_2@C_{92}$	16	126339	C_s	17.1	0.84
$Er_2C_2@C_{90}$	**21**	**99893**	**C_1**	**19.1**	**1.39**
$Er_2C_2@C_{90}$	**44**	**99916**	**C_2**	**20.1**	**0.90**
$Er_2C_2@C_{90}$	45	99917	C_2	22.0	1.11
$Er_2C_2@C_{90}$	22	99894	C_1	25.7	1.13
$Er_2C_2@C_{90}$	23	99895	C_2	27.4	1.28
$Er_2C_2@C_{90}$	10	99882	C_s	31.3	1.12
$Er_2C_2@C_{90}$	38	99910	C_1	31.7	1.12
$Er_2C_2@C_{90}$	19	99891	C_2	34.7	0.88
$Er_2C_2@C_{90}$	36	99908	C_{2v}	38.3	0.97

Natural electron configuration analyses of $Er_2C_2@C_{90}$ isomers under study. As for Er element, it has a [Xe]$4f^{12}6s^2$ electronic configuration. Natural electron configuration analyses on the four isomers reveal that three electrons consisting of two 6*s* electrons and one *f* electron are formally transferred from each Er atom (Table S8), thus, presenting the trivalent oxidation state. In addition, 2*p* electrons on the inner carbon atoms rise to ~3, indicating that one electron may transfer from Er atoms to these 2*p* orbitals and result in the negatively charged atoms. Therefore, their electronic configurations can be represented as $(Er^{3+})_2(C_2)^{2-}@(C_{90})^{4-}$, i.e., four electrons are formally transferred to carbon cages from the inner Er_2C_2 cluster.

Table S8. Natural electron configuration populations and NPA charges of Er atoms and carbon atoms in $Er_2C_2@C_2(43)$-C_{90}, $Er_2C_2@C_2(40)$-C_{90}, $Er_2C_2@C_2(44)$-C_{90}, and $Er_2C_2@C_1(21)$-C_{90}.

Isomer	Atom	NPA Charge	Populations
$Er_2C_2@C_2(43)$-C_{90}	Er91	1.262	$6s^{0.16}4f^{11.09}5d^{0.98}6p^{0.40}6d^{0.12}$
	Er92	1.474	$6s^{0.12}4f^{11.11}5d^{0.86}6p^{0.30}6d^{0.10}7p^{0.05}$
	C93	-0.279	$2s^{1.30}2p^{2.95}3s^{0.02}3p^{0.02}3d^{0.02}$
	C94	-0.704	$2s^{1.20}2p^{3.48}3p^{0.02}$

$Er_2C_2@C_2(40)$-C_{90}	Er91	1.240	$6s^{0.12}4f^{11.11}5d^{0.86}6p^{0.41}6d^{0.13}7p^{0.02}$
	Er92	1.317	$6s^{0.16}4f^{11.11}5d^{0.89}6p^{0.40}6d^{0.11}7p^{0.02}$
	C93	-0.415	$2s^{1.27}2p^{3.11}3p^{0.02}3d^{0.02}$
	C94	-0.503	$2s^{1.26}2p^{3.20}3p^{0.02}3d^{0.02}$
$Er_2C_2@C_2(44)$-C_{90}	Er91	1.294	$6s^{0.16}4f^{11.13}5d^{0.92}6p^{0.22}6d^{0.13}7p^{0.02}$
	Er92	1.266	$6s^{0.16}4f^{11.11}5d^{0.94}6p^{0.32}6d^{0.13}7p^{0.12}$
	C93	-0.385	$2s^{1.26}2p^{3.08}3p^{0.02}3d^{0.02}$
	C94	-0.522	$2s^{1.26}2p^{3.23}3p^{0.02}3d^{0.02}$
$Er_2C_2@C_1(21)$-C_{90}	Er91	1.303	$6s^{0.16}4f^{11.12}5d^{0.90}6p^{0.40}6d^{0.12}7p^{0.02}$
	Er92	1.246	$6s^{0.17}4f^{11.10}5d^{0.94}6p^{0.32}6d^{0.13}7p^{0.12}$
	C93	-0.343	$2s^{1.26}2p^{3.04}3p^{0.02}3d^{0.02}$
	C94	-0.540	$2s^{1.26}2p^{3.24}3s^{0.02}3p^{0.02}3d^{0.02}$

Table S9. Distances (*d*, in Å), delocalization indices (DI), and BCP parameters[a] for the Er-C and C-C bonds in the four isomers.

Bond	d	DI	ρ_{bcp}	$\nabla^2\rho_{bcp}$	H_{bcp}	$\lvert V_{bcp}\rvert/G_{bcp}$	G_{bcp}/ρ_{bcp}
$Er_2C_2@C_2(43)$-C_{90}							
C93-C94	1.254	1.735	0.405	-1.343	-0.553	3.544	/
Er92-C94	2.293	1.131	0.078	0.187	-0.022	1.318	0.878
Er91-C93	2.274	1.313	0.070	0.215	-0.016	1.234	1.008
Er92-C2	2.455	0.618	0.051	0.188	-0.006	1.109	1.033
Er92-C34	2.446	0.665	0.054	0.168	-0.009	1.169	0.935
Er92-C35	2.449	0.668	0.055	0.173	-0.009	1.165	0.945
Er92-C41	2.441	0.670	0.055	0.174	-0.009	1.167	0.950
Er91-C56	2.432	0.673	0.056	0.175	-0.009	1.177	0.950
Er91-C65	2.442	0.658	0.055	0.176	-0.009	1.164	0.960
Er91-C66	2.545	0.602	0.045	0.153	-0.004	1.086	0.938
C94-C4	3.803	0.002	0.004	0.010	0.000	0.822	/
C93-C90	3.229	0.018	0.009	0.027	0.001	0.779	/
$Er_2C_2@C_2(40)$-C_{90}							
C93-C94	1.250	1.454	0.403	-1.314	-0.546	3.511	/
Er91-C94	2.382	1.058	0.057	0.178	-0.010	1.180	0.949
Er92-C93	2.383	1.109	0.059	0.197	-0.008	1.142	0.975
Er91-C69	2.408	0.680	0.058	0.194	-0.010	1.170	1.011
Er91-C79	2.406	0.686	0.058	0.194	-0.010	1.174	1.005

Er92-C19	2.419	0.681	0.058	0.181	-0.010	1.183	0.961
Er92-C20	2.422	0.678	0.057	0.183	-0.010	1.178	0.969
C93-C24	3.846	0.003	0.003	0.009	0.000	0.786	0.590
C93-C9	3.745	0.002	0.004	0.010	0.000	0.836	0.527
C94-C41	3.650	0.005	0.004	0.013	0.001	0.791	0.596
C94-C8	3.764	0.002	0.003	0.010	0.000	0.781	0.592
C94-C58	3.684	0.002	0.004	0.011	0.000	0.822	0.553
$Er_2C_2@C_2(44)$-C_{90}							
C93-C94	1.243	1.439	0.402	-1.297	-0.543	3.480	/
Er91-C94	2.304	1.145	0.066	0.201	-0.015	1.229	0.982
Er92-C93	2.381	1.089	0.059	0.195	-0.008	1.148	0.970
Er91-C37	2.400	0.674	0.059	0.192	-0.011	1.180	0.996
Er92-C66	2.445	0.665	0.055	0.168	-0.009	1.177	0.933
Er92-C81	2.467	0.649	0.052	0.161	-0.008	1.161	0.926
Er92-C70	2.488	0.638	0.050	0.165	-0.006	1.134	0.941
C93-C62	4.091	0.001	0.002	0.007	0.000	0.759	/
C94-C87	3.747	0.005	0.006	0.015	0.001	0.823	/
C94-C88	3.459	0.008	0.006	0.016	0.001	0.785	/
$Er_2C_2@C_1(21)$-C_{90}							
C93-94	1.234	1.445	0.402	-1.302	-0.544	3.491	/
Er92-C94	2.398	0.968	0.059	0.194	-0.008	1.141	0.960
Er91-C94	2.344	1.053	0.063	0.193	-0.012	1.198	0.964
Er92-C59	2.404	0.696	0.059	0.183	-0.011	1.198	0.959
Er91-C21	2.411	0.685	0.058	0.181	-0.011	1.193	0.961
Er91-C36	2.415	0.683	0.058	0.184	-0.011	1.187	0.970
C93-C5	3.753	0.005	0.003	0.010	0.000	0.782	/
C94-C38	3.391	0.011	0.006	0.018	0.001	0.789	/

[a] The unit of all BCPs' parameters is a.u..

Table S10. The details of the vis-NIR absorptions of $Er_2C_2@C_{90}$ isomers.[a]

Compound	Vis-NIR absorption bands (nm)	Onset (nm)	Optical bandgap (eV)[a]
$Er_2C_2@C_2(43)$-C_{90}	474, 522, 563, 647, 776, 864	1018	1.22
$Er_2C_2@C_2(40)$-C_{90}	464, 552, 657, 822, 976, 1145	1415	0.88
$Er_2C_2@C_2(44)$-C_{90}	474, 641, 705, 822, 1304, 1560	1736	0.71
$Er_2C_2@C_1(21)$-C_{90}	596, 713, 877, 1051	1564	0.79

[a]Optical bandgap (eV) ≈ 1240/onset (nm).

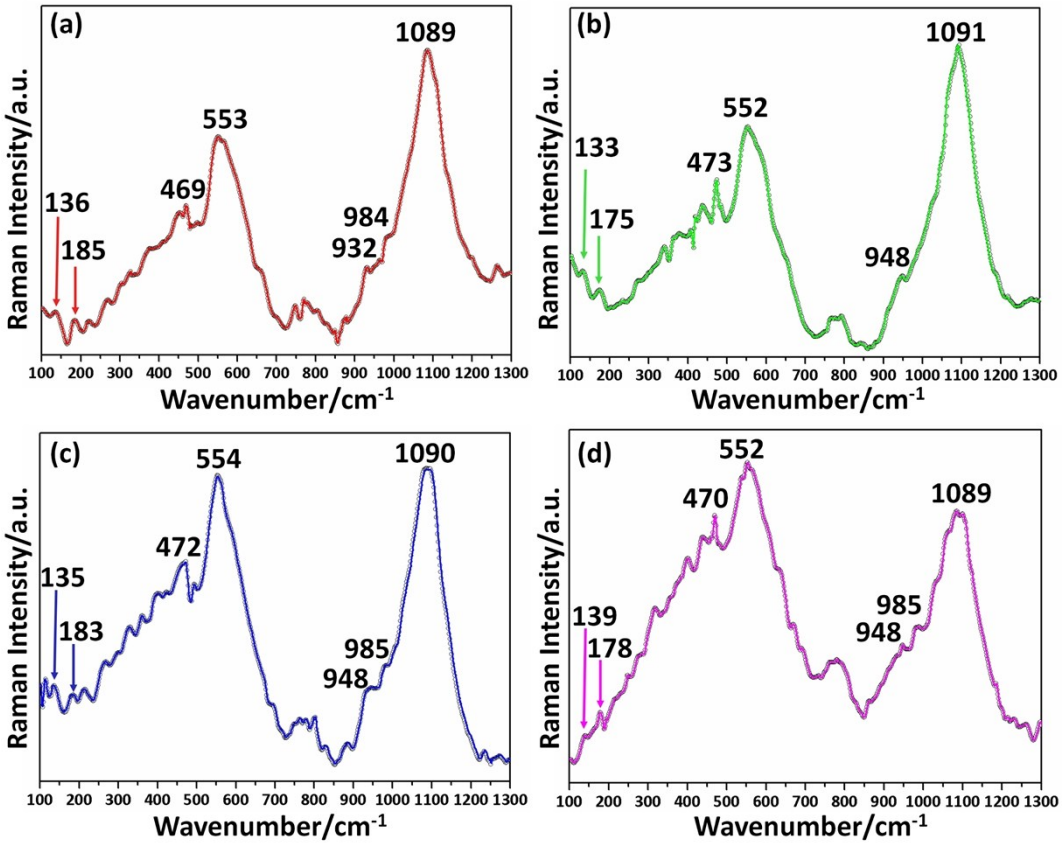

Fig. S4 Low-energy Raman spectra of (a) $Er_2C_2@C_2(43)$-C_{90}, (b) $Er_2C_2@C_2(40)$-C_{90}, (c) $Er_2C_2@C_2(44)$-C_{90}, and (d) $Er_2C_2@C_1(21)$-C_{90} at 532 nm excitation.

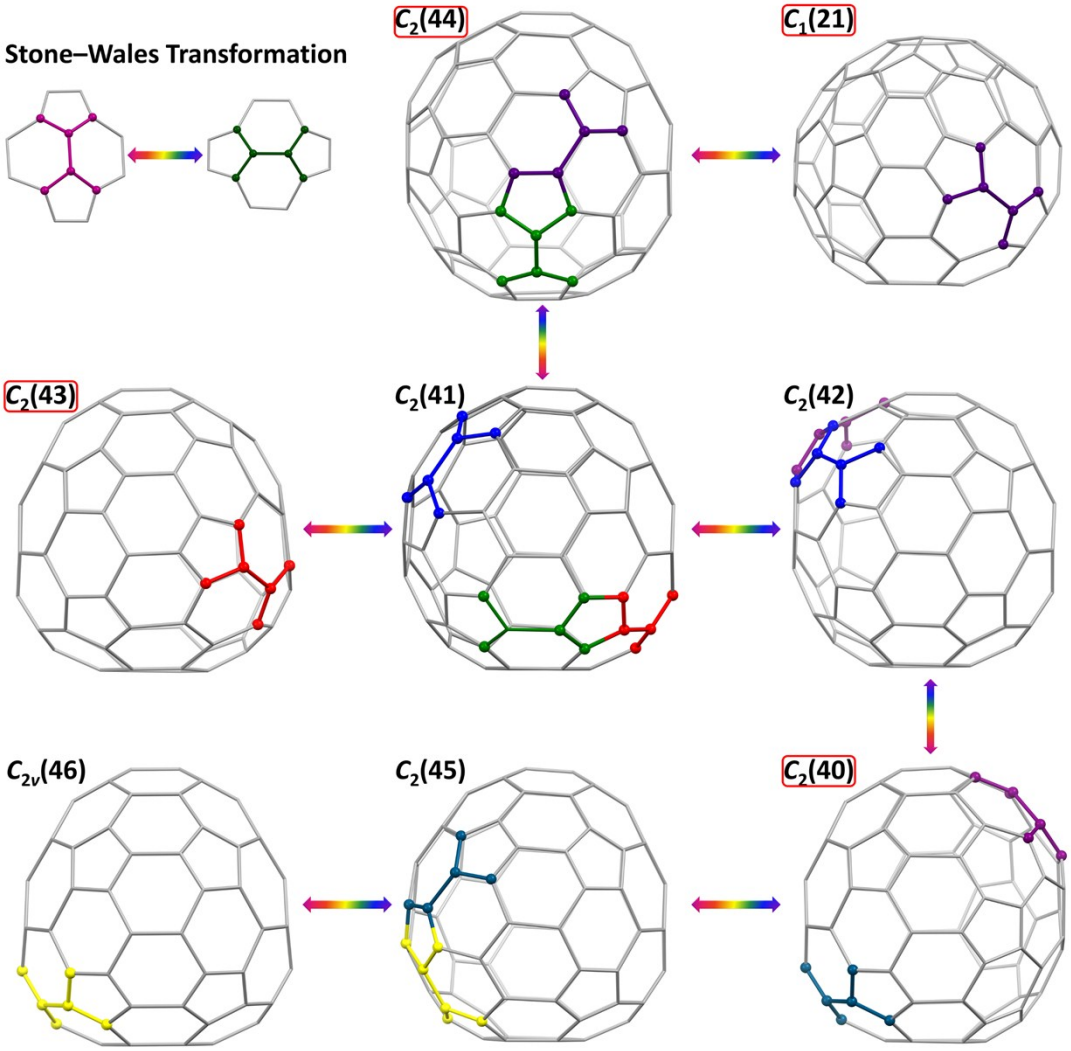

Fig. S5 Transformations among the eight reported IPR C_{90}-cages with C_2(41)-C_{90} as the starting point. The rearrangement pathways are related by one-step Stone-Wales transformation.[18] The cages reported in this work are highlighted with red boxes. Multiple color codes are used to enhance visualization.

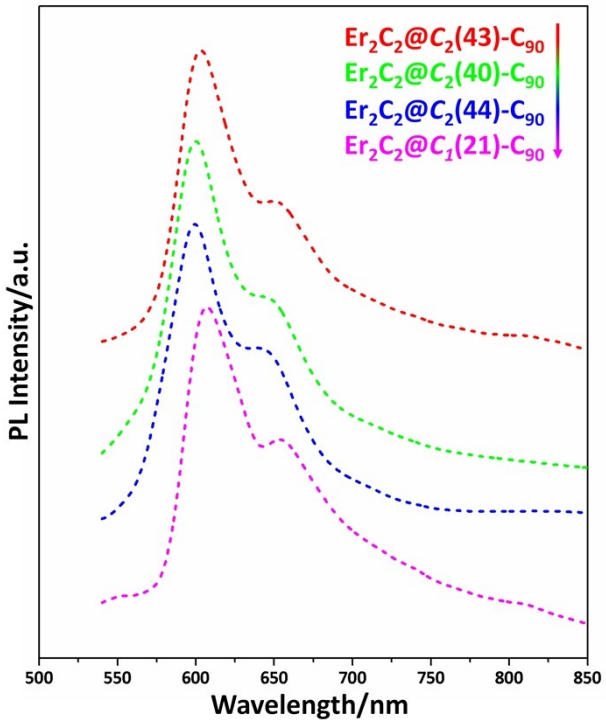

Fig. S6 PL spectra of the $Er_2C_2@C_{90}$ isomers solid powder upon excitation at 532 nm at room temperature. The curves are vertically shifted for ease of comparison.

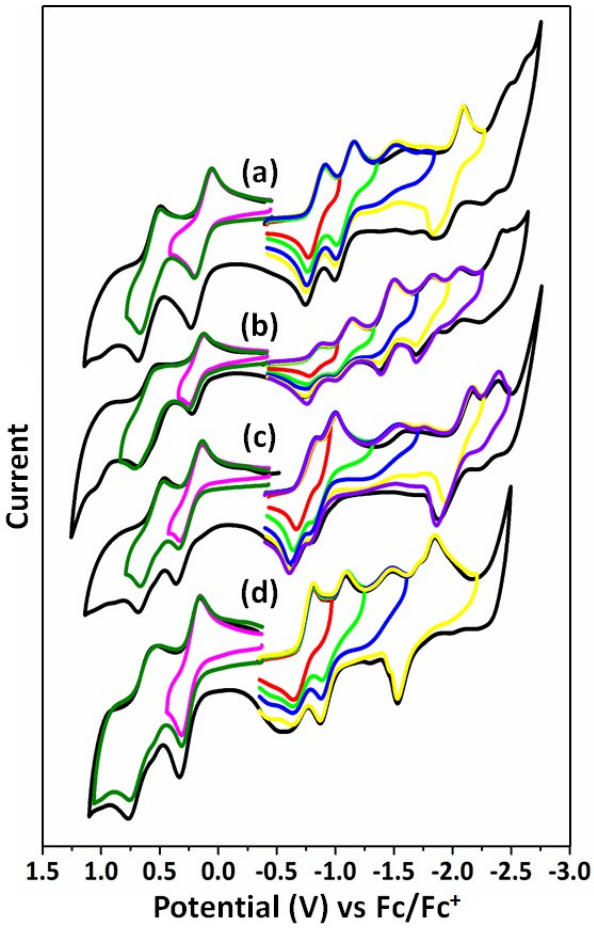

Fig. S7 Cyclic voltammograms of (a) $Er_2C_2@C_2(43)$-C_{90}, (b) $Er_2C_2@C_2(40)$-C_{90}, (c) $Er_2C_2@C_2(44)$-C_{90}, and (d) $Er_2C_2@C_1(21)$-C_{90} in 0.05 M $TBAPF_6$/o-DCB solution, (scan

rate: 100 mV s^{-1}).

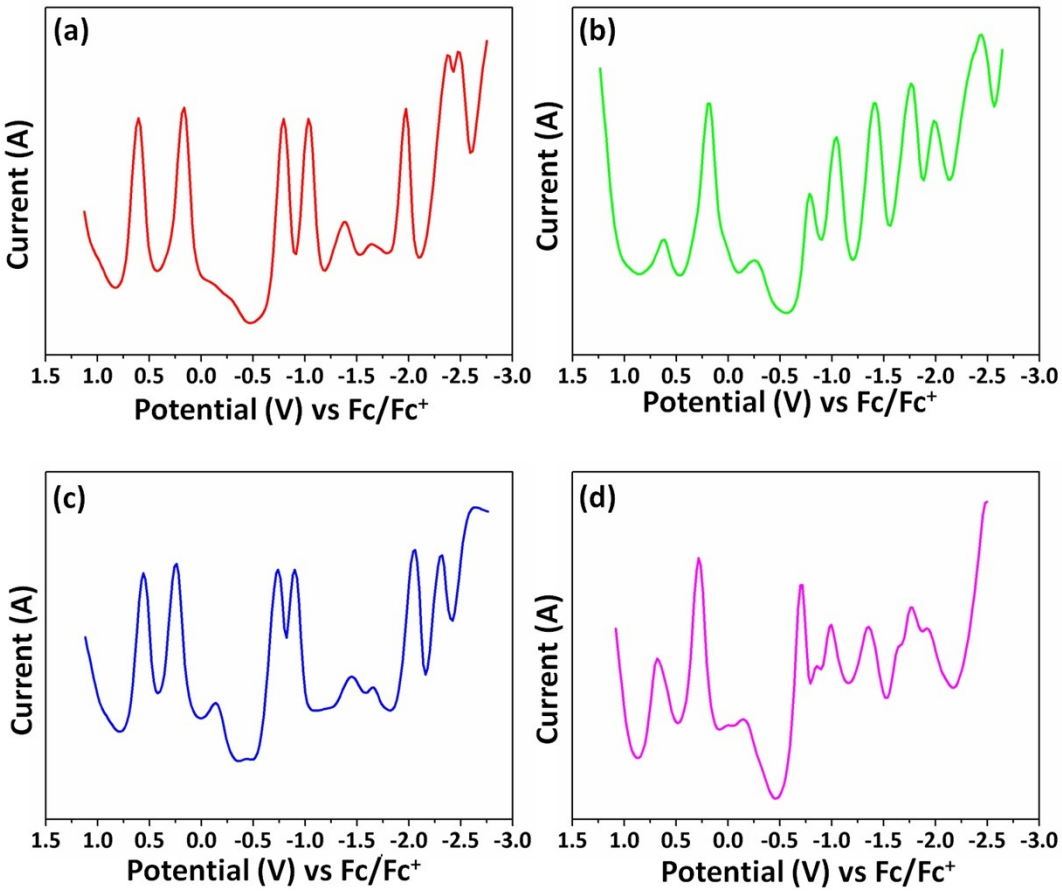

Fig. S8 DPV curves of (a) $Er_2C_2@C_2(43)$-C_{90}, (b) $Er_2C_2@C_2(40)$-C_{90}, (c) $Er_2C_2@C_2(44)$-C_{90}, and (d) $Er_2C_2@C_1(21)$-C_{90}. Conditions: working electrode, glassy carbon; counter electrode, Pt wire; reference electrode, Ag wire; supporting electrolyte, 0.05 M $TBAPF_6$ in o-DCB; pulse amplitude, 50 mV; pulse width, 50 ms; pulse period, 500 ms; scan rate, 20 mV s^{-1}.

References:

1. Krätschmer, W.; Lamb, L. D.; Fostiropoulos, K.; Huffman, D. R., Solid C_{60}: a new form of carbon. *Nature* **1990,** *347* (6291), 354-358.

2. Wang, Q.-S.; Zhang, K.-H.; Cui, Y.; Wang, Z.-J.; Pan, Q.-Y.; Liu, K.; Sun, B.; Zhou, H.; Li, M.-J.; Xu, Q.; Xu, C.-Y.; Yu, F.; He, J.-H., Upgrade of macromolecular crystallography beamline BL17U1 at SSRF. *Nuclear Science and Techniques* **2018,** *29* (5), 68.

3. Sheldrick, G. M., SHELXT - Integrated space-group and crystal-structure determination. *Acta Crystallographica a-Foundation and Advances* **2015,** *71*, 3-8.

4. Becke, A. D., Density-functional exchange-energy approximation with correct asymptotic behavior. *Physical Review A* **1988,** *38* (6), 3098-3100.

5. Becke, A. D., Density-functional thermochemistry. III. The role of exact exchange. *The Journal of Chemical Physics* **1993,** *98* (7), 5648-5652.

6. Lee, C.; Yang, W.; Parr, R. G., Development of the Colle-Salvetti correlation-energy formula into a functional of the electron density. *Physical Review B* **1988,** *37* (2), 785-

789.
7. Yang, H.; Jin, H.; Zhen, H.; Wang, Z.; Liu, Z.; Beavers, C. M.; Mercado, B. Q.; Olmstead, M. M.; Balch, A. L., Isolation and Crystallographic Identification of Four Isomers of Sm@C_{90}. *Journal of the American Chemical Society* **2011,** *133* (16), 6299-6306.
8. Wang, J.; Zhao, Y.-y.; Lee, P.-H.; Irle, S., Er^{3+} Photoluminescence in $Er_2@C_{82}$ and $Er_2C_2@C_{82}$ Metallofullerenes Elucidated by Density Functional Theory. *Inorganic Chemistry* **2017,** *56* (11), 6576-6583.
9. Andrae, D.; Häußermann, U.; Dolg, M.; Stoll, H.; Preuß, H., Energy-adjustedab initio pseudopotentials for the second and third row transition elements. *Theoretica chimica acta* **1990,** *77* (2), 123-141.
10. Schwerdtfeger, P.; Dolg, M.; Schwarz, W. H. E.; Bowmaker, G. A.; Boyd, P. D. W., Relativistic effects in gold chemistry. I. Diatomic gold compounds. *The Journal of Chemical Physics* **1989,** *91* (3), 1762-1774.
11. Cao, X.; Dolg, M., Segmented contraction scheme for small-core lanthanide pseudopotential basis sets. *Journal of Molecular Structure: Theochem* **2002,** *581* (1), 139-147.
12. Slanina, Z.; Uhlík, F.; Feng, L.; Akasaka, T.; Lu, X.; Adamowicz, L., Calculations of the $Lu_3N@C_{80}$ two-isomer equilibrium. *Fullerenes, Nanotubes and Carbon Nanostructures* **2019,** *27* (5), 382-386.
13. Zhao, P.; Zhao, X.; Ehara, M., Theoretical Insight into Sc_2C_{76}: Carbide Clusterfullerene $Sc_2C_2@C_{74}$ versus Dimetallofullerene $Sc_2@C_{76}$. *Inorganic Chemistry* **2017,** *56* (17), 10195-10203.
14. Zhao, P.; Zhao, X.; Ehara, M., Theoretical Insights into Monometallofullerene $Th@C_{76}$: Strong Covalent Interaction between Thorium and the Carbon Cage. *Inorganic Chemistry* **2018,** *57* (6), 2961-2964.
15. Zhao, P.; Li, M.-Y.; Guo, Y.-J.; Zhao, R.-S.; Zhao, X., Single Step Stone-Wales Transformation Linking Two Thermodynamically Stable $Sc_2O@C_{78}$ Isomers. *Inorganic Chemistry* **2016,** *55* (5), 2220-2226.
16. Yang, T.; Zhao, X.; Osawa, E., Can a Metal-Metal Bond Hop in the Fullerene Cage? *Chemistry - A European Journal* **2011,** *17* (37), 10230-10234.
17. M. J. Frisch, G. W. Trucks, H. B. Schlegel, G. E. Scuseria, M. A. Robb, J. R. Cheeseman, G. Scalmani, V. Barone, B. Mennucci, G. A. Petersson, H. Nakatsuji, M. Caricato, X. Li, H. P. Hratchian, A. F. Izmaylov, J. Bloino, G. Zheng, J. L. Sonnenberg, M. Hada, M. Ehara, K. Toyota, R. Fukuda, J. Hasegawa, M. Ishida, T. Nakajima, Y. Honda, O. Kitao, H. Nakai, T. Vreven, J. A. Montgomery, Jr., J. E. Peralta, F. Ogliaro, M. Bearpark, J. J. Heyd, E. Brothers, K. N. Kudin, V. N. Staroverov, R. Kobayashi, J. Normand, K. Raghavachari, A. Rendell, J. C. Burant, S. S. Iyengar, J. Tomasi, M. Cossi, N. Rega, J. M. Millam, M. Klene, J. E. Knox, J. B. Cross, V. Bakken, C. Adamo, J. Jaramillo, R. Gomperts, R. E. Stratmann, O. Yazyev, A. J. Austin, R. Cammi, C. Pomelli, J. W. Ochterski, R. L. Martin, K. Morokuma, V. G. Zakrzewski, G. A. Voth, P. Salvador, J. J. Dannenberg, S. Dapprich, A. D. Daniels, Ö. Farkas, J. B. Foresman, J. V. Ortiz, J. Cioslowski and D. J. Fox, *Gaussian 09, Revision E.01*, Gaussian, Inc., Wallingford CT, 2013.

18. Stone, A. J.; Wales, D. J., Theoretical studies of icosahedral C_{60} and some related species. *Chemical Physics Letters* **1986,** *128* (5), 501-503.